

Light Higgs channel of the resonant decay of magnon condensate in superfluid $^3\text{He-B}$

V. V. Zavjalov,^{1,*} S. Autti,¹ V. B. Eltsov,¹ P. J. Heikkinen,¹ and G. E. Volovik^{1,2}

¹*Low Temperature Laboratory, Department of Applied Physics,
Aalto University, PO Box 15100, FI-00076 AALTO, Finland*

²*Landau Institute for Theoretical Physics, acad. Semyonov av., 1a, 142432, Chernogolovka, Russia*
(Dated: March 3, 2022)

In superfluids the order parameter, which describes spontaneous symmetry breaking, is an analogue of the Higgs field in the Standard Model of particle physics. Oscillations of the field amplitude are massive Higgs bosons, while oscillations of the orientation are massless Nambu-Goldstone bosons. The 125 GeV Higgs boson, discovered at Large Hadron Collider, is light compared to electroweak energy scale, which led to a suggestion of the “little Higgs” extension of the Standard Model, in which the light Higgs appears as a NG mode acquiring mass due to violation of a hidden symmetry. Here we show that such light Higgs exists in superfluid $^3\text{He-B}$, where one of three Nambu-Goldstone spin-wave modes acquires small mass due to the spin-orbit interaction. Other modes become optical and acoustic magnons. We observe parametric decay of Bose-Einstein condensate of optical magnons to light Higgs modes and decay of optical to acoustic magnons. Formation of a light Higgs from a Nambu-Goldstone mode observed in $^3\text{He-B}$ opens a possibility that such scenario can be realized in other systems, where violation of some hidden symmetry is possible, including the Standard Model.

PACS numbers: 67.30.H-, 14.80.Bn, 67.30.hj, 67.85.Fg

Introduction

The superfluid transition in ^3He , a fermionic isotope of helium, occurs due to formation of Cooper pairs with orbital momentum $L = 1$ and spin $S = 1$. The corresponding order parameter is a 3×3 matrix of complex numbers, which includes both spin and orbital degrees of freedom.¹ Thus, besides fermionic quasiparticles, superfluid ^3He possesses 18 bosonic degrees of freedom, collective modes (oscillations) of the order parameter. Each mode has a relativistic spectrum $\omega^2(k) = \omega_0^2 + (ck)^2$, with a mode-specific wave velocity c and a gap (or mass) ω_0 . Modes with non-zero ω_0 are Higgs modes and others are Nambu-Goldstone (NG) modes. Each NG mode corresponds to spontaneously broken continuous symmetry of the normal state.

In conventional superconductors with the order parameter of a single complex number, only the symmetry with respect to the change of the wave-function phase is broken. This leads to one NG phase mode and one amplitude Higgs mode, which was experimentally observed.²⁻⁴

In unconventional B phase of superfluid ^3He the symmetry with respect to relative rotations of the spin and orbital spaces is additionally broken,⁵ and the order parameter in the zero magnetic field is

$$A_{\alpha i} = \Delta e^{i\Phi} R_{\alpha i}(\hat{\mathbf{n}}, \theta), \quad (1)$$

where Δ is the gap in the fermionic spectrum, Φ is the phase and $R_{\alpha i}$ is a rotation matrix, which connects spin and orbital degrees of freedom. The matrix $R_{\alpha i}$ is represented in terms of the rotation axis $\hat{\mathbf{n}}$ and angle θ . Parameters Φ , $\hat{\mathbf{n}}$ and θ determine a 4-dimensional subspace of degenerate states. Thus among 18 collective modes of $^3\text{He-B}$, Fig. 1a, four are NG modes: oscillation of Φ is sound and oscillations of $R_{\alpha i}$ (or $\hat{\mathbf{n}}$ and θ) are spin waves. The other 14 modes are the Higgs modes with energy

gaps of the order of Δ . These heavy Higgs modes have been investigated for a long time both theoretically⁶⁻⁹ and experimentally.¹⁰⁻¹⁴

In superconductors and in the Standard Model, the NG bosons become massive due to the Anderson-Higgs mechanism.¹⁵⁻¹⁷ In electrically neutral ^3He these modes are gapless, when viewed from the scale of $\Delta \sim 100$ MHz (set by the critical temperature $T_c \sim 10^{-3}$ K). At low energy scale of ~ 1 MHz, corresponding to the frequency of our nuclear magnetic resonance (NMR) experiments, two weak effects become significant: spin-orbit interaction and applied magnetic field \mathbf{H} , Fig. 1b.

Spin-orbit interaction lifts the degeneracy with respect to θ , and the minimum energy corresponds to the so-called Leggett angle $\theta_L = \arccos(-1/4)$. This explicit violation of the symmetry of the B phase leads to appearance of the gap for the θ mode. This mode becomes an additional, light, Higgs boson. The gap value Ω_B is called Leggett frequency, it is a measure of the spin-orbit interaction. At low temperatures $\Omega_B \sim 100$ kHz $\ll \Delta$.

Two other spin-wave modes are oscillations of $\hat{\mathbf{n}}$. In the magnetic field the equilibrium state corresponds to $\hat{\mathbf{n}} \parallel \mathbf{H}$ and the field splits these two modes in the same way as in ferromagnets. One of the modes, the optical magnon, acquires the gap equal to the Larmor frequency $\omega_L = \gamma H$ (where γ is the gyromagnetic ratio). Another one, the acoustic magnon, remains gapless, but its spectrum becomes quadratic. Such unusual form of the spectrum comes from a violation of the time reversal symmetry by the magnetic field (general discussion of the NG modes with quadratic spectrum see in Ref. 18).

All three low frequency spin-wave modes are described by the closed system of Leggett equations.¹ In particle physics such set of low-energy modes, which includes NG modes and a light Higgs, is called the Little Higgs field.¹⁹ Formal definition of such field in $^3\text{He-B}$ is given in Sup-

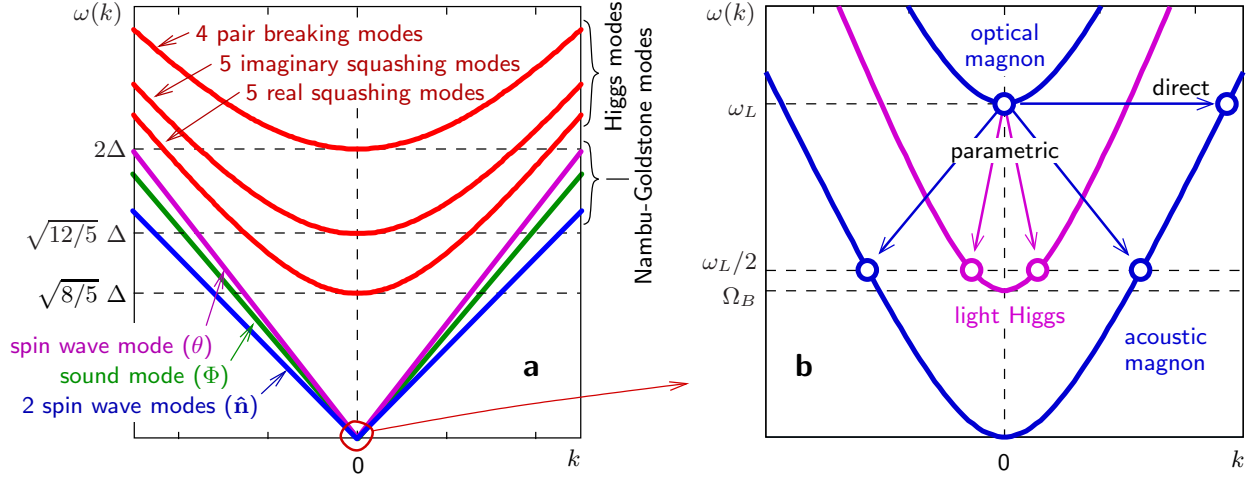


FIG. 1: **Illustration of collective-mode spectra in $^3\text{He-B}$.** (a) Modes at high energy scale ($\omega \sim \Delta \sim 100$ MHz). From top to bottom there are six separate branches. Three red lines show heavy Higgs modes: four degenerate pair breaking modes with the gap 2Δ , five imaginary squashing modes with the gap $\sqrt{12/5}\Delta$, five real squashing modes with the gap $\sqrt{8/5}\Delta$. Nambu-Goldstone modes include a sound mode (propagating oscillations of Φ), a spin-wave mode which corresponds to propagating oscillations of θ , two spin-wave modes which corresponds to propagating oscillations of \hat{n} . These modes are gapless at the high energy scale and have different propagation velocities c . (b) Spin-waves modes at low energy scale ($\omega \sim 10^{-3}\Delta \sim 100$ kHz). Due to spin-orbit interaction the θ mode acquires a small gap $\Omega_B \ll \Delta$ and becomes a light Higgs boson. Two \hat{n} modes are split by the magnetic field into optical and acoustic magnons. Arrows indicate decay channels observed in our experiments.

plementary Note 1.

Results

In an NMR experiment one follows the dynamics of magnetization \mathbf{M} , or of the spin \mathbf{S} of the sample. The motion of θ , corresponds to longitudinal spin waves, $\delta\mathbf{S} \parallel \mathbf{H}$, while oscillations of \hat{n} correspond to transverse spin motion, $\delta\mathbf{S} \perp \mathbf{H}$. Optical magnons can be directly created with traditional transverse NMR. With a suitable coil system one can also directly excite longitudinal spin oscillations, or light Higgs mode.²⁰ Coupling to short-wavelength acoustic magnons is hard to achieve in a traditional NMR experiment with large excitation coils.

In this work we use a technique, based on Bose-Einstein condensate (BEC) of optical magnons,²¹ to probe interaction and conversion between all components of the little Higgs field in $^3\text{He-B}$. As a result, we observe parametric decay of optical magnons to light Higgs bosons, and both parametric and direct conversion between optical and acoustic magnons. The measured mass of light Higgs and propagation velocity of acoustic magnons are close to the expected values. Thus we experimentally confirm the little Higgs scenario in $^3\text{He-B}$. The little Higgs field appears in quantum chromodynamics,²² where NG modes (pions) acquire light mass due to the explicit violation of the chiral symmetry, which is negligible at high energy, but becomes significant at low energy.²³ The relatively small mass of the 125 GeV Higgs boson observed at the Large Hadron Collider suggests that it might be also the pseudo-Goldstone (light Higgs) boson (see e.g. Ref. 24 and references therein).

Suhl instability. As a tool to study dynamics of the little Higgs field in superfluid $^3\text{He-B}$ we use trapped Bose-Einstein condensates of optical magnons, Fig. 2. The

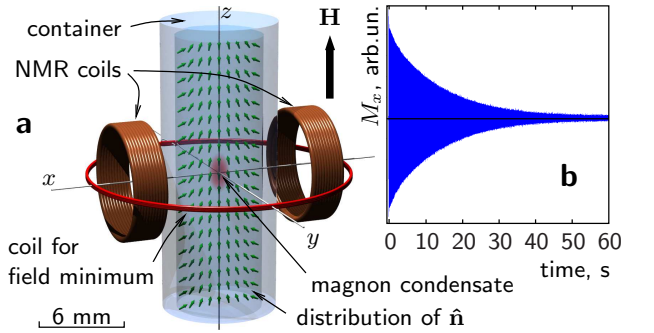


FIG. 2: **Experimental setup.** (a) Superfluid $^3\text{He-B}$ is confined in a cylindrical quartz container, and a constant magnetic field \mathbf{H} is applied along the container axis. A special coil creates a minimum of the field magnitude H in the axial direction, while transverse NMR coils are used to pump optical magnons and to detect magnetization precession. Green arrows show equilibrium distribution of the \hat{n} vector, which together with the \mathbf{H} profile creates a trap for optical magnons near the axis of the sample. In this trap magnon BEC is formed. (b) An example of the signal from the NMR coil during the condensate decay measured at $\omega/2\pi = 833$ kHz and $P = 0$ bar. Its amplitude is proportional to the coherently precessing transverse magnetization of the condensate.

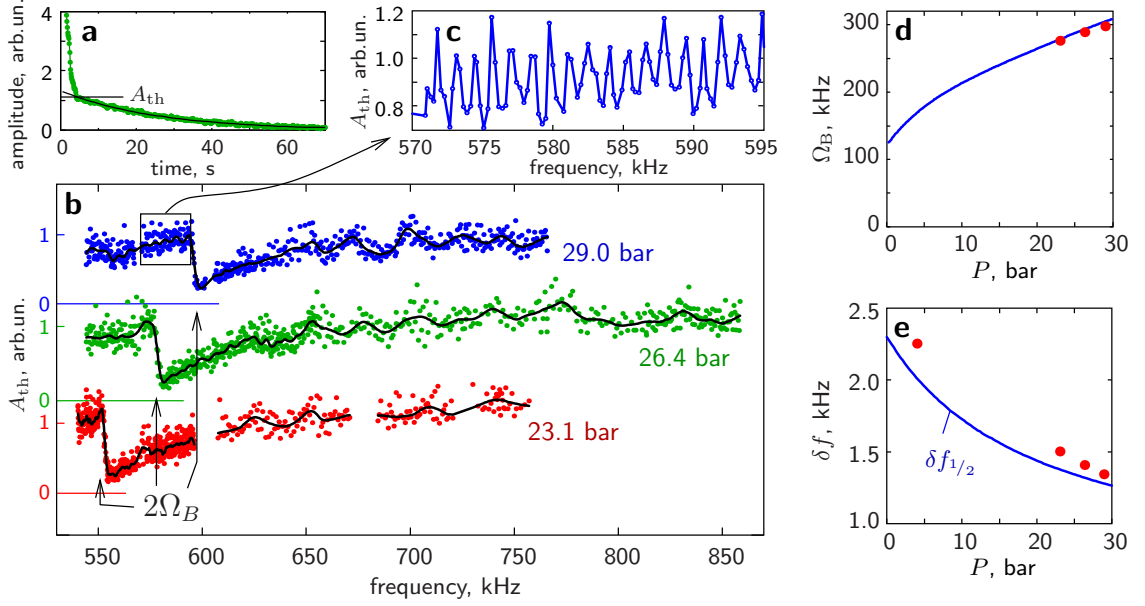


FIG. 3: **Measurements of the Suhl instability.** (a) An example measurement of the NMR signal amplitude during the magnon condensate decay obtained at $\omega_L/2\pi = 741$ kHz and $P = 26.4$ bar. A Suhl instability threshold at the amplitude A_{th} is clearly seen. (b) Dependence of the threshold amplitude A_{th} on the frequency of optical magnons $\omega_{opt} \approx \omega_L$ (colored symbols) for three pressures P . Sharp decrease is seen at $\omega_{opt} = 2\Omega_B(P)$, where the decay of an optical magnon to two light Higgs bosons becomes possible. Black lines are smoothed data using running average. Curves for different pressures are shifted in the vertical direction and respective zero levels are marked by horizontal lines. (c) Zoom to one measurement in the panel b shows periodic modulation, which corresponds to resonances of acoustic magnons in the experimental container. (d) Pressure dependence of the light Higgs boson mass Ω_B (symbols) from measurements in the panel b. (e) Frequency separation of acoustic magnon resonances (symbols) from measurements like in the panel c. Solid lines in the panels d and e are theoretical values based on known ^3He parameters¹ without fitting.

condensate is well separated from the container walls, where the strongest magnetic relaxation in ^3He usually occurs.²⁵ Thus tiny relaxation effects, connected to coupling of optical magnons to other components of the little Higgs field, can be observed.

When number of pumped magnons is low, slow exponential relaxation of the precession signal is determined by spin diffusion and energy losses in the NMR pick-up circuit,²⁶ Fig. 2b. We have found that above some threshold amplitude the relaxation becomes much faster, Fig. 3a. The explanation is the Suhl instability,²⁷ a well-known nonlinear effect in magnets when a uniform precession of magnetization (here at the optical magnon frequency ω_{opt}) parametrically excites a pair of acoustic magnons with twice smaller frequency ω_{ac} and opposite \mathbf{k} -vectors: $\omega_{opt} = \omega_{ac}(\mathbf{k}) + \omega_{ac}(-\mathbf{k})$. In the case of ^3He -B both acoustic magnons and the light Higgs modes can be parametrically excited, Fig. 1b. The process occurs with conservation of energy and momentum. The threshold amplitude is inversely proportional to the coupling between decaying and excited waves and proportional to the relaxation in the excited wave.

Mass of light Higgs. The measured threshold amplitude as a function of NMR frequency and pressure is plotted in Fig. 3b. The frequency dependence al-

lows us to identify the decay channels. It is clear from Fig. 1b that the decay of the optical magnon to a pair of light Higgs bosons with the frequency ω_{Higgs} , $\omega_{opt} = \omega_{Higgs}(\mathbf{k}) + \omega_{Higgs}(-\mathbf{k})$, is possible only when the precession frequency is larger than $2\Omega_B$. We see a pronounced drop of the threshold amplitude at this frequency: The threshold decreases by about an order of magnitude.

In Fig. 3d the measured mass of light Higgs Ω_B is plotted as a function of pressure. Measurements are in a good agreement with values of the Leggett frequency from Ref. 1.

Resonances of acoustic magnons. In addition to the sharp drop, connected with light Higgs mode, we find periodic modulation of the threshold amplitude as a function of the frequency of the precession, Fig. 3c. These periodic peaks originate from the parametric decay of the optical magnons in the BEC to acoustic magnons. The frequency dependence is explained by quantization of the magnon spectrum in the cylindrical container, which serves as a resonator for acoustic magnons. Consider a decay of the optical magnon with frequency ω_{opt} into acoustic magnons with frequency $\omega_{ac} = N\omega_{opt}$, where for the parametric excitation $N = 1/2$. In the following discussion we will use $\omega_{opt} = \omega_L$ since the difference is negligible for trapped optical magnons. By sweeping the

magnetic field we can change both magnon spectrum and magnon trap and observe resonances in the cell. The simple resonance condition for acoustic magnons in a cylinder with the radius R gives the distance between the resonances (Supplementary Note 2):

$$\delta f_N = \frac{1}{\sqrt{N(1+N)}} \frac{c}{4R}. \quad (2)$$

where c is the relevant spin-wave velocity.

In Fig. 3e the measured acoustic magnon resonance period $\delta f_{1/2}$ is plotted as a function of pressure. The results are in a good agreement with Eq. (2), where values of the spin-wave velocity are taken from our recent measurements.⁴

Effect of quantized vortices. An additional relaxation mechanism for the magnon condensate is found when quantized vortices are formed in the sample. In the presence of these localized topological objects the momentum \mathbf{k} of the spin-wave modes is not conserved, and one expects direct excitation of acoustic magnons by the optical mode. We can rotate the sample with angular velocities up to $\Omega = 2$ radian per second to create a cluster of rectilinear quantized vortices, which cross the whole experimental region including the magnon BEC, Fig. 4a. In this state the relaxation rate, plotted as a function of the frequency in Fig. 4b, reveals several periodic sets of peaks. We attribute these peaks to resonances of acoustic magnons with frequencies ω_L , $2\omega_L$, etc.

In $^3\text{He-B}$ the rotational symmetry of a vortex is spontaneously broken and the vortex core can be treated as a bound state of two half-quantum vortices which can rotate around the vortex axis. Dynamics of the vortex is affected by the precessing magnetization^{30,31}. Precession of \mathbf{S} and $\hat{\mathbf{n}}$ in the magnon BEC produces torsional oscillations of the vortex core. The fact that the equilibrium position of $\hat{\mathbf{n}}$ deviates from the vertical direction within the magnon BEC makes this oscillations unharmonic. As a result, acoustic magnons with frequencies $N\omega_L$ can be emitted.

The amplitudes of the various resonances depend on a distribution of vortex cores and the wave nodes of acoustic magnons. For example, an axially symmetric distribution of vortices can excite only symmetric waves, which means doubling of the observed resonance period. In our experiment acoustic magnons (with wave length $5 - 10 \mu\text{m}$) are emitted by vortices, which are within the magnon condensate. The distance between vortices $0.1 - 0.2 \text{ mm}$ is comparable with the size of the trapped condensate $0.2 - 0.4 \text{ mm}$. Thus the amplitudes of resonances are sensitive to details, such as order parameter texture, rotation and pressure and we do not see all the harmonics at all pressures. Nevertheless the resonance periods plotted in Fig. 4c follow the theoretical values (2) or their multiples (denoted as $2\delta f_1$, etc.).

Discussion

To summarize, we have observed the interplay of all three spin wave modes, which form a little Higgs field in superfluid $^3\text{He-B}$. In particular, we have found two channels of parametric decay of optical magnons: to a pair of light Higgs bosons and to a pair of acoustic magnons. While the search for similar resonant production of pairs of Standard Model Higgs bosons reported by the ATLAS collaboration³² has not succeeded yet, our results support the basic physical idea behind this effort. Another system where the light Higgs mode can be observed is the multicomponent condensate in cold gases³³, where interaction between components can be set up to produce the hidden symmetry.

We find that the low-energy physics in superfluid ^3He has many common features of the Higgs scenario in Standard Model: both are described by the $\text{SU}(2)$ and $\text{U}(1)$ symmetry groups; the acoustic and optical magnons cor-

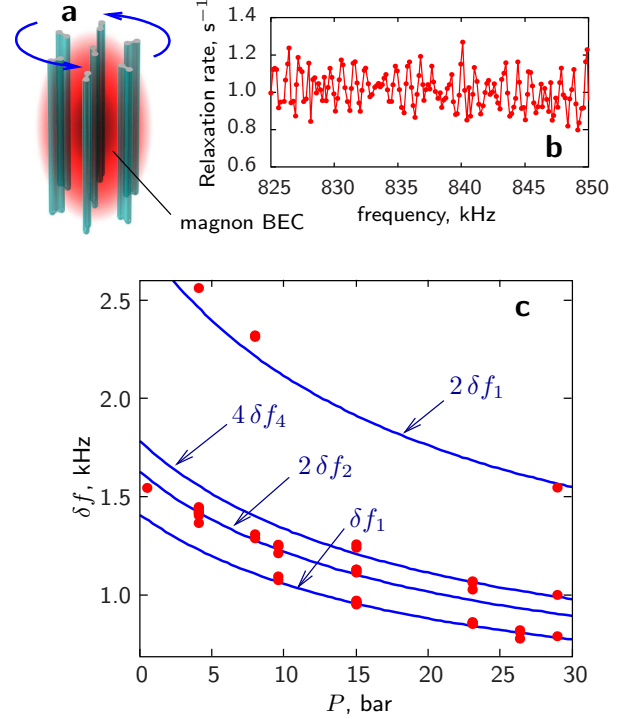


FIG. 4: Excitation of acoustic magnons by vortices. (a) Schematic plot of vortices in rotating $^3\text{He-B}$. Precession of magnetization of the magnon condensate cause oscillations of non-axisymmetric vortex cores. The oscillations produce acoustic magnons and increase relaxation of the condensate. (b) Relaxation rate of the magnon condensate as a function of frequency, measured at $\Omega = 1$ radian per second and $P = 23.4$ bar. Two sets of acoustic magnon resonances with periods about 1 kHz produce a clearly seen beat with a period of 5 kHz. (c) Measured periods of magnon condensate relaxation peaks (symbols) as a function of pressure. Lines are plotted using equation (2) for acoustic magnon resonances without fitting parameters.

respond to the doublet of W^+ and W^- gauge bosons which spectrum also splits in magnetic field;³ the light Higgs mode has parallel with the 125 GeV Higgs boson. However, in addition, the $^3\text{He-B}$ has the high-energy sector with 14 heavy Higgs modes. This suggests that in the same manner the 125 GeV Higgs boson belongs to the low energy sector of particle physics, and if so, one may expect the existence of the heavy Higgs bosons at TeV scale.

We have demonstrated that the short-wavelength acoustic magnons can be emitted and detected with the BEC of optical magnons. Acoustic magnons can be lensed by non-uniform magnetic fields and the order-parameter texture, and thus might serve in future as a powerful local probe to study topological superfluidity of ^3He , including Majorana fermions on the boundaries of the superfluid and in the cores of quantized vortices.

Methods

The sample geometry and NMR setup. Superfluid $^3\text{He-B}$ is placed in a cylindrical container with the inner diameter of $2R = 5.85$ mm, made from fused quartz, Fig. 2. The container has closed top end and open bottom end, which provides the thermal contact to the nuclear demagnetization refrigerator. Static magnetic field is applied parallel to the container axis. A special coil creates a controlled minimum of the field magnitude along the axial direction. Transverse NMR coils, made from copper wire, are used to create and detect magnetization precession. Coils are part of a tuned tank circuit with the Q value of around 130. Frequency tuning is provided by a switchable capacitance bank, installed at the mixing chamber of the dilution refrigerator. To improve signal to noise ratio, we use a cold preamplifier, thermalized to liquid helium bath.

The measurements are performed at low temperatures $T < 0.2 T_c$, where spin-wave velocities and the Leggett frequency are temperature-independent. Typically we use $T = 130 - 350 \mu\text{K}$, depending on pressure. The temperature is measured by a quartz tuning fork thermometer, installed

at the bottom of the sample cylinder. The heat leak to the sample was measured in earlier work to be about 12 pW .³⁵ The measurements are performed at pressures $0 - 29$ bar and in magnetic fields $H = 17 - 26$ mT with corresponding NMR frequencies $\omega_L/2\pi = 550 - 830$ kHz.

Magnon trap. Minimum of the axial magnetic field forms a trapping potential for optical magnon quasiparticles in the axial direction. Trapping in the radial direction is provided by the spin-orbit interaction via the equilibrium distribution of the order parameter. In this geometry it forms the so-called flare-out texture: $\hat{\mathbf{n}}$ is parallel to \mathbf{H} on the cell axis and tilted near walls because of boundary conditions.³⁶ The combined magneto-textural trap is nearly harmonic with trapping length about 0.3 mm in the radial direction and 1 mm in the axial direction (see Supplementary Note 3 for details).

Measurements of magnon BEC. Owing to the geometry, the coils couple only to optical magnons with $k \approx 0$. With a short rf pulse in the NMR coils non-equilibrium optical magnons are created. At temperatures of our experiment equilibration within the magnon subsystem proceeds much faster than the decay of magnon number, and the pumped magnons are condensed to the ground level of the trap within 0.1 s from the pulse. Manifestation of Bose-Einstein condensation is the spontaneously coherent precession of the condensate magnetization,^{37,38} which induces current in the NMR coils. The amplified signal is recorded by a digital oscilloscope; an example record is in Fig. 2b. We then perform sliding Fourier transform of the signal with the window $0.3 - 1$ s. In the resulting sharp peak in the spectrum the frequency determines the BEC precession frequency ω_{opt} , while the amplitude (such as shown in Fig. 3a) is proportional to the square root of the number of magnons in the trap.

Rotation. The sample is installed in the rotating nuclear demagnetization refrigerator ROTA,³⁹ and can be put in rotation together with the cryostat and the measuring equipment. The cryostat is properly balanced and suspended on active vibration isolation, and in rotation the heat leak to the sample remains below 20 pW .³⁵ Vortices are created by increasing angular velocity Ω from zero to a target value at temperature around $0.7 T_c$, where the mutual friction allows for fast relaxation of vortex configuration towards an equilibrium array.⁴⁰ Further cool-down is performed in rotation.

* Electronic address: vladislav.zavyalov@aalto.fi

¹ Vollhardt, D. & Wölfle, P. *The superfluid phases of helium 3*, Taylor and Francis, London (1990).

² Matsunaga, R. *et al.* The Higgs amplitude mode in BCS superconductors $\text{Nb}_{1-x}\text{Ti}_x\text{N}$ induced by terahertz pulse excitation. *Phys. Rev. Lett.* **111**, 057002 (2013).

³ Matsunaga, R. *et al.* Light-induced collective pseudospin precession resonating with Higgs mode in a superconductor. *Science* **345**, 1145–1149 (2014).

⁴ Sherman, D. *et al.* The Higgs mode in disordered superconductors close to a quantum phase transition. *Nature Phys.* **11**, 188–192 (2015).

⁵ Leggett, A.J. A theoretical description of the new phases of liquid ^3He , *Rev. Mod. Phys.* **47**, 331–414 (1975).

⁶ Vdovin, Y.A. in: *Applications of Methods of Quantum Field Theory to Many Body Problems*, ed. A.I. Alekseyeva (GOS

ATOM IZDAT, Moscow, 1963).

⁷ Maki, K. Propagation of zero sound in the Balian-Werthamer state. *J. Low Temp. Phys.* **16**, 465–477 (1974).

⁸ Nagai, K. Collective excitations from the Balian-Werthamer state. *Prog. Theor. Phys.* **54**, 1–18 (1975).

⁹ Tewordt, L. & Einzel, D. Collective modes and gap equations for the superfluid states in ^3He . *Phys. Lett. A* **56**, 97–98 (1976).

¹⁰ Giannetta, R. *et al.*, Observation of a New Sound Attenuation Peak in Superfluid $^3\text{He-B}$. *Phys. Rev. Lett.* **45**, 262–265 (1980);

¹¹ Mast, D. *et al.*, Measurements of High-Frequency Sound Propagation in $^3\text{He-B}$. *Phys. Rev. Lett.* **45**, 266–269 (1980).

¹² Avenel, O., Varoquaux, E. & Ebisawa, H. Field splitting of the new sound attenuation peak in $^3\text{He-B}$. *Phys. Rev. Lett.* **45**, 1952–1955 (1980).

- ¹³ Movshovich, R., Varoquaux, E., Kim, N. & Lee, D.M. Splitting of the squashing collective mode of superfluid $^3\text{He-B}$ by a magnetic field. *Phys. Rev. Lett.* **61**, 1732–1735 (1988).
- ¹⁴ Collett, C. A., Pollanen, J., Li, J. I. A., Gannon, W. J. & Halperin, W. P. Zeeman splitting and nonlinear field-dependence in superfluid ^3He . *J. Low Temp. Phys.* **171**, 214–219 (2013).
- ¹⁵ Higgs, P.W. Broken Symmetries and the Masses of Gauge Bosons. *Phys. Rev. Lett.* **13**, 508–509 (1964).
- ¹⁶ Anderson, P. W. Plasmons, gauge invariance, and mass. *Phys. Rev.* **130**, 439–442 (1963).
- ¹⁷ Pekker D. & Varma, C.M. Amplitude/Higgs modes in condensed matter physics. *Annu. Rev. Condens. Matter Phys.* **6** 269–297 (2015).
- ¹⁸ Nitta, M. & Takahashi, D.A. Quasi-Nambu-Goldstone modes in nonrelativistic systems. *Phys. Rev. D* **91**, 025018 (2015).
- ¹⁹ Schmaltz, M. & Tucker-Smith, D. Little Higgs Review. *Ann. Rev. Nucl. Part. Sci.* **55**, 229–270 (2005).
- ²⁰ Osheroff, D. D. Longitudinal and Transverse Resonance in the B Phase of Superfluid ^3He . *Phys. Rev. Lett.* **33**, 1009–1012 (1974).
- ²¹ Bunkov, Yu. M. & Volovik, G. E. Spin superfluidity and magnon BEC. *International Series of Monographs on Physics* **156**, Volume 1, 253–311 (2013).
- ²² Dobrescu, B.A. & Frugiuele, C. Hidden GeV-scale interactions of quarks. *Phys. Rev. Lett.* **113**, 061801 (2014).
- ²³ Weinberg, S. Approximate symmetries and pseudo-Goldstone bosons. *Phys. Rev. Lett.* **29**, 1698–1701 (1972).
- ²⁴ Volovik, G.E. & Zubkov, M.A. Scalar excitation with Leggett frequency in $^3\text{He-B}$ and the 125 GeV Higgs particle in top quark condensation models as pseudo-Goldstone bosons. *Phys. Rev. D* **92**, 055004 (2015).
- ²⁵ Fisher, S. N., Pickett, G. R., Skyba, P. & Suramlshvili, N. Decay of persistent precessing domains in $^3\text{He-B}$ at very low temperatures. *Phys. Rev. B* **86**, 024506 (2012).
- ²⁶ Heikkinen, P.J., Autti, S., Eltsov, V.B., Haley, R.P. & Zavjalov, V.V. Microkelvin thermometry with Bose-Einstein condensates of magnons and applications to studies of the AB interface in superfluid ^3He . *J. Low Temp. Phys.* **175**, 681–705 (2014).
- ²⁷ Suhl, H. The theory of ferromagnetic resonance at high signal powers. *J. Phys. Chem. Solids* **1**, 209–227 (1957).
- ²⁸ Thuneberg, E.V. Hydrostatic theory of superfluid $^3\text{He-B}$. *J. Low Temp. Phys.* **122**, 657–682 (2001).
- ²⁹ Zavjalov, V.V., Autti, S., Eltsov, V.B. & Heikkinen, P.J. Measurements of the anisotropic mass of magnons confined in a harmonic trap in superfluid $^3\text{He-B}$. *JETP Letters* **101**, 802–807 (2015).
- ³⁰ Kondo, Y. *et al.* Direct observation of the nonaxisymmetric vortex in superfluid $^3\text{He-B}$. *Phys. Rev. Lett.* **67**, 81–84 (1991).
- ³¹ Silaev, M.A., Thuneberg, E.V. & Fogelström, M. Lifshitz transition in the double-core vortex in $^3\text{He-B}$. arXiv:1505.02136 (2015).
- ³² Aad, G. *et al.* (ATLAS Collaboration) Search for Higgs boson pair production in the $\gamma\gamma b\bar{b}$ final state using pp collision data at $\sqrt{s} = 8$ TeV from the ATLAS detector. *Phys. Rev. Lett.* **114**, 081802 (2015).
- ³³ Ueda M., *Fundamentals and New Frontiers of Bose-Einstein Condensation*. World Scientific, 2010.
- ³⁴ Chernodub, M.N. Superconducting properties of vacuum in strong magnetic field, *Int. J. Mod. Phys. D* **23**, 1430009 (2014).
- ³⁵ Hosio J.J. *et al.* Propagation of thermal excitations in a cluster of vortices in superfluid $^3\text{He-B}$. *Phys. Rev. B* **84**, 224501 (2011).
- ³⁶ Smith, H., Brinkman, W. F. & Engelsberg, S. Textures and NMR in superfluid $^3\text{He-B}$. *Phys. Rev. B* **15**, 199–213 (1977).
- ³⁷ Cousins, D.J., Fisher, S.N., Gregory, A.I., Pickett, G.R. & Shaw, N.S. Persistent coherent spin precession in superfluid $^3\text{He-B}$ driven by off-resonant excitation. *Phys. Rev. Lett.* **82**, 4484–4487 (1999).
- ³⁸ Autti, S. *et al.* Self-trapping of magnon Bose-Einstein condensates in the ground state and on excited levels: From harmonic to box confinement. *Phys. Rev. Lett.* **108**, 145303 (2012).
- ³⁹ Hakonen, P.J. *et al.*, Rotating nuclear demagnetization refrigerator for experiments on superfluid He^3 . *Cryogenics* **23**, 243–250 (1983).
- ⁴⁰ Eltsov, V.B., Hänninen, R. & Krusius, M. Quantum turbulence in superfluids with wall-clamped normal component. *Proc. Natl. Acad. Sci. USA* **111**, 4711–4718 (2014).

Acknowledgements

We thank M. Krusius and V.S L'vov for useful discussions. This work has been supported in part by the EU 7th Framework Programme (FP7/2007-2013, Grant No. 228464 Mikrokkelvin), by the Academy of Finland (project no. 284594), and by the facilities of the Cryohall infrastructure of Aalto University. P.J.H. acknowledges financial support from the Väisälä Foundation of the Finnish Academy of Science and Letters, and S.A. that from the Finnish Cultural Foundation.

Author contributions

The experiments were conducted by S.A., P.J.H., V.V.Z., and V.B.E., the theoretical analysis was carried out by G.E.V. and V.V.Z., the paper was written by V.V.Z., G.E.V. and V.B.E., with contribution from all the authors.

Conflicting financial interests

The authors declare no competing financial interests.

SUPPLEMENTARY NOTE 1

Spin waves in $^3\text{He-B}$

Spin waves in $^3\text{He-B}$ correspond to motions of the rotation matrix R_{aj} . The matrix can be represented by means of the rotation axis $\hat{\mathbf{n}}$ and the rotation angle θ as

$$R_{aj} = \cos \theta \delta_{aj} + (1 - \cos \theta) n_a n_j - \sin \theta e_{ajk} n_k. \quad (3)$$

The motion is affected by the energy of the spin-orbit interaction F_{so} and the gradient energy F_{∇} :

$$F_{\text{so}} = \frac{\chi_B \Omega_B^2}{15\gamma^2} (R_{jj} R_{kk} + R_{jk} R_{kj}), \quad (4)$$

$$F_{\nabla} = \frac{1}{2} \Delta^2 (K_1 G_1 + K_2 G_2 + K_3 G_3), \quad (5)$$

where

$$\begin{aligned} G_1 &= \nabla_j R_{ak} \nabla_j R_{ak}, \\ G_2 &= \nabla_j R_{ak} \nabla_k R_{aj}, \\ G_3 &= \nabla_j R_{aj} \nabla_k R_{ak}, \end{aligned}$$

χ_B is the spin susceptibility of the $^3\text{He-B}$, γ the gyromagnetic ratio for the ^3He atom, Ω_B the Leggett frequency, Δ the superfluid gap, and K_1, K_2 and K_3 are parameters of the gradient energy.

The spin-orbit interaction energy has a simple form in terms of $\hat{\mathbf{n}}$ and θ with a minimum at $\theta = \arccos(-1/4)$:

$$F_{\text{so}} = \frac{\chi_B \Omega_B^2}{15\gamma^2} (\cos \theta + 1/4)^2 + \text{const}. \quad (6)$$

The equation of small spin oscillations near the equilibrium value $\mathbf{S}^0 = (\chi_B/\gamma) \mathbf{H}$ is²

$$\begin{aligned} \ddot{\mathbf{S}}_c &= [\dot{\mathbf{S}} \times \gamma \mathbf{H}]_c \\ &+ \frac{\Delta^2 \gamma^2}{\chi_B} [K \nabla^2 \mathbf{S}_c - K' \nabla_j R_{cj}^0 R_{ak}^0 \nabla_k \mathbf{S}_a] \\ &- \Omega_B^2 \hat{\mathbf{n}} \cdot (\mathbf{S} - \mathbf{S}^0) \hat{\mathbf{n}}_c, \end{aligned} \quad (7)$$

where $K = 2K_1 + K_2 + K_3$ and $K' = K_2 + K_3$.

In a texture with $\hat{\mathbf{n}} \parallel \mathbf{H}$ or in a high magnetic field $\omega_L^2/\Omega_B^2 \gg 1$ one can separate transverse and longitudinal oscillations. In the case of short wavelengths (when the spin changes on a much shorter distance than the texture) one can write the quasiclassical spectra for plane waves:

$$\begin{aligned} c_{\perp}^2 k^2 + (c_{\parallel}^2 - c_{\perp}^2)(\mathbf{k} \cdot \hat{\mathbf{l}})^2 + \frac{1}{2} \Omega_B^2 \sin^2 \beta_n &= \omega(\omega - \omega_L), \\ C_{\perp}^2 k^2 + (C_{\parallel}^2 - C_{\perp}^2)(\mathbf{k} \cdot \hat{\mathbf{l}})^2 + \Omega_B^2 \cos^2 \beta_n &= \omega^2, \end{aligned} \quad (8)$$

where β_n is an angle between $\hat{\mathbf{n}}$ and \mathbf{H} , the orbital anisotropy axis $\hat{\mathbf{l}}_j = R_{aj} \mathbf{S}_a^0$ and the spin wave velocities are introduced as

$$\begin{aligned} c_{\perp}^2 &= \frac{\gamma^2 \Delta^2}{\chi_B} (K - K'/2), \quad c_{\parallel}^2 = \frac{\gamma^2 \Delta^2}{\chi_B} K, \\ C_{\perp}^2 &= \frac{\gamma^2 \Delta^2}{\chi_B} K, \quad C_{\parallel}^2 = \frac{\gamma^2 \Delta^2}{\chi_B} (K - K'). \end{aligned} \quad (9)$$

The spin wave velocities are anisotropic, they have different values if the wave propagates in the direction of $\hat{\mathbf{l}}$ or in the perpendicular direction. The second line of Supplementary

equation (8) describes a longitudinal wave, the light Higgs mode with a “relativistic” spectrum

$$\omega_{\text{Higgs}} = \sqrt{\Omega_B^2 + (C k)^2}. \quad (10)$$

The first line of Supplementary equation (8) describes two modes of transverse waves, optical and acoustic magnons, with spectra of the form:

$$\omega_{\text{opt}} = \frac{\omega_L}{2} + \sqrt{\left(\frac{\omega_L}{2}\right)^2 + (c k)^2}, \quad \omega_{\text{ac}} = -\frac{\omega_L}{2} + \sqrt{\left(\frac{\omega_L}{2}\right)^2 + (c k)^2}. \quad (11)$$

In Supplementary equations (10) and (11) the effects of anisotropy and of the spin-orbit interaction are omitted for simplicity.

Little Higgs field for spin waves in $^3\text{He-B}$

Let us introduce a vector field

$$\mathbf{n} = \hat{\mathbf{n}} \sin \theta/2. \quad (12)$$

The spin-orbit interaction (6) provides a “Mexican Hat” potential for the \mathbf{n} -field

$$F_{\text{so}} = \Lambda(|\mathbf{n}|^2 - n_0^2)^2. \quad (13)$$

where $n_0^2 = 5/8$ and parameter $\Lambda = \frac{32}{15} \frac{\chi_B}{\gamma^2} \Omega_B^2$.

In the terminology of particle physics the \mathbf{n} -vector serves as the “little Higgs” field. In the vacuum states the amplitude of the field is fixed, $|\mathbf{n}| = n_0$, while they are degenerate with respect to the orientation of $\hat{\mathbf{n}}$. The broken $SU(2)$ symmetry leads to two Nambu-Goldstone modes (propagating oscillations of the orientation of $\hat{\mathbf{n}}$), and one light Higgs mode (propagating oscillations of the amplitude $|\mathbf{n}|$ around n_0). These three modes comprising the little Higgs field are similar to the bosonic sector of Standard Model, where also the $SU(2)$ symmetry is instrumental. This low energy sector of Standard Model contains the NG modes (the gauge bosons) and one “light Higgs” (the 125 GeV Higgs boson). Our two Nambu-Goldstone spin-wave modes correspond to the doublet of the W-bosons. The spectrum of the spin wave modes in $^3\text{He-B}$ splits in magnetic field into acoustic and optical modes. The similar splitting is discussed for the spectrum of the W-bosons in magnetic field (see e.g. Ref.³). Moreover, in strong magnetic fields the Bose condensation of the W-bosons is expected, which is similar to the Bose condensation of optical magnons.

SUPPLEMENTARY NOTE 2

Resonance condition for acoustic magnons

Let's consider an excitation of acoustic magnons with frequency $N\omega_L$. Here $N = 1/2$ corresponds to the parametric excitation, $N = 1, 2, \dots$ to the excitation of acoustic magnons with frequency $\omega_L, 2\omega_L, \dots$. The resonances observed in the experiments correspond to standing waves in the cylindrical cell with radius R . For the short spin waves the resonances can be treated in the quasiclassical approximation:

$$2 \int_0^R k_r dr = n\pi, \quad (14)$$

where k_r is the classical trajectory along the cell diameter and n is integer quantum number. This quantization corresponds to the wave modes in cylinder with high radial and small azimuthal quantum numbers.

The effect of the spin-orbit interaction on the spectrum of short-wave acoustic magnons can be neglected, but anisotropy of wave velocity is important. The ratio of the velocities for $\mathbf{k} \parallel \hat{\mathbf{l}}$ and $\mathbf{k} \perp \hat{\mathbf{l}}$ is $c_{\parallel}/c_{\perp} \approx \sqrt{4/3}$. Substituting the transverse magnon spectrum (8) without the spin-orbit term into (14) and taking into account that $\omega = N\omega_L$ we get

$$\omega_L = \frac{1}{\sqrt{N(1+N)}} \frac{\pi n c}{2R} \quad (15)$$

where c is a harmonic mean velocity in the non-uniform texture:

$$1/c = \frac{1}{R} \int_0^R (c_{\perp}^2 + (c_{\parallel}^2 - c_{\perp}^2) \sin^2 \beta_l(r))^{-1/2} dr, \quad (16)$$

and β_l is an angle between $\hat{\mathbf{l}}$ and \mathbf{H} .

The distance between the resonances is:

$$\delta f_N = \frac{1}{2\pi} \frac{\partial \omega_L}{\partial n} = \frac{1}{\sqrt{N(1+N)}} \frac{c}{4R}. \quad (17)$$

Note that the spin wave spectra (8) have been obtained with the assumption of zero coupling between transverse and longitudinal modes ($\omega^2/\Omega_B^2 \gg 1$ or $\beta_n \ll 1$). In our experiment this condition is approximately valid for directly excited magnons with $\omega > 2\Omega_B$. We use the same approximation also for parametrically excited magnons with $\omega \approx \Omega_B$. This is probably the reason why the agreement of the experimental data with Eq. (17) is much better for the directly excited magnons.

SUPPLEMENTARY NOTE 3

Trap for magnon quasiparticles

In the case of optical magnons with $\omega \approx \omega_L$, localized in the center of the cell, where $\hat{\mathbf{n}}$ is almost parallel to \mathbf{H} ,

equation (7) can be rewritten in a form of a Schrödinger equation for magnon quasiparticles, where complex value $s_+ = \frac{1}{\sqrt{2}}(S_x + iS_y)$ plays role of the wave function and precession frequency ω plays role of the energy. Effect of texture on the gradient terms is neglected here because it adds only a small correction to the total gradient energy.

$$\left[-\frac{c_{\perp}^2}{\omega_L} (\nabla_x^2 + \nabla_y^2) - \frac{c_{\parallel}^2}{\omega_L} \nabla_z^2 + \frac{\Omega_B^2}{2\omega_L} \sin^2 \beta_n + \omega_L \right] s_+ = \omega s_+ \quad (18)$$

Non-uniform potential for magnons is formed by the order parameter texture and the magnetic field (β_n and ω_L parameters).

$$U = \frac{\Omega_B^2}{2\gamma H} \sin^2 \beta_n + \omega_L. \quad (19)$$

In our setup the potential has a quadratic minimum in the center of the sample: in the flare-out texture angle β_n near the sample axis is linear, $\beta_n = \beta'_n r$ and magnetic field of the longitudinal coil has also quadratic profile near the center.

We use pulsed NMR to populate a few lowest levels in this harmonic trap. If the number of magnons in the system is small enough, interaction between the levels is negligible and the excited states can be resolved in the measurements independently. If the magnon population is above a certain threshold, they collapse to the ground state and form a Bose-Einstein condensate.

From the spectra of the magnon levels in the trap we can find values of spin-wave velocities c_{\perp} and c_{\parallel} . This work is presented in Ref. 4.

* Electronic address: vladislav.zavjalov@aalto.fi

SUPPLEMENTARY REFERENCES

- ¹ Thuneberg, E.V. Hydrostatic theory of superfluid $^3\text{He-B}$. *J. Low Temp. Phys.* **122**, 657–682 (2001).
- ² Theodorakis, S. & Fetter, A.L. Vortices and NMR in rotat-

- ing $^3\text{He-B}$. *J. Low Temp. Phys.* **52**, 559–591 (1983).
- ³ Chernodub, M.N. Superconducting properties of vacuum in strong magnetic field, *Int. J. Mod. Phys. D* **23**, 1430009 (2014).
- ⁴ Zavjalov, V.V., Autti, S., Eltsov, V.B. & Heikkinen, P.J. Measurements of the anisotropic mass of magnons confined in a harmonic trap in superfluid $^3\text{He-B}$. *JETP Letters* **101**, 802–807 (2015).